Soft magnetism in mechanically alloyed nanocrystalline materials

T. D. Shen,* R. B. Schwarz, and J. D. Thompson
Materials Science and Technology Division, Mail Stop G755, Los Alamos National Laboratory, Los Alamos, New Mexico 87545, USA
(Received 15 April 2005; published 14 July 2005)

We study the magnetic properties of nanocrystalline $Fe_{80}Cu_{20}$ (at. %) and $Fe_{92}Al_2Si_6$ (wt %) alloy powders prepared by mechanical alloying. Although these powders have crystallite sizes of approximately 10 nm, their coercivity is rather high, 20–30 Oe. We demonstrate that the main contribution to the coercivity in mechanically alloyed powders arises from the long-range fluctuations in the residual stress, which couples to total anisotropy factor via the magnetostriction of the alloy. The residual stress can be partially reduced by annealing within a narrow temperature range. We have modified the "random anisotropy model" to take into account the residual stress in the mechanically alloyed nanocrystalline powders.

DOI: 10.1103/PhysRevB.72.014431 PACS number(s): 75.50.Kj, 75.75.+a, 75.50.Bb, 61.46.+w

I. INTRODUCTION

It has been long known that large-grained polycrystalline ferromagnetic materials (grain sizes D typically ranging from ~ 10 μm to 1 mm) can be magnetically soft, with coercivity below approximately 1 Oe. For large grains the magnetic structure is multidomain and friction to domain motion arises from inclusions and residual stresses rather than from grain boundaries. As the grain size decreases, the main contribution to the coercivity arises from grain boundaries. Thus, fine-grained materials are usually magnetically harder than coarse-grained materials of the same composition, purity, and internal stress.

In 1988, Yoshizawa *et al.* showed[1] that nanocrystalline Fe-Cu-Nb-Si-B alloys ($D \sim 10$ nm) are magnetically soft. This behavior does not follow the above-mentioned domain pinning model. Since then, numerous studies have been performed to investigate the soft magnetic properties of nanostructured materials.[2,3] Herzer,[4] following an earlier "random anisotropy model" set forth to explain soft ferromagnetism in amorphous alloys,[5] suggested that soft ferromagnetism should also be found in crystalline alloys whenever the grain size is smaller than the magnetic exchange length L_{ex}. In this case, fluctuations in magnetic anisotropy on the length scale of the grain size are irrelevant to domain wall pinning. According to this model, H_C follows a D^6-power law, a relationship which has been verified by Herzer[2] for several Fe-based nanocrystalline alloys prepared by annealing their amorphous precursors.

Two methods have been used to prepare nanocrystalline materials: (1) crystallization of rapidly quenched amorphous ribbons[2,3,6] and (2) mechanical alloying (MA).[7] Although the nanocrystalline materials prepared by the first method have soft magnetic properties, this method has various shortcomings: (a) due to the high cooling rates required to quench the melt into a glass, the amorphous precursors can usually be prepared only as thin ribbons (<50 μm); (b) the alloy compositions of these ribbons are usually limited to those of deep eutectics; (c) the nanocrystalline materials prepared by crystallizing amorphous precursors are usually brittle. The second method does not have some of these limitations. The main advantage of the MA method is that one is not limited to the compositions of deep eutectics. In principle, the nanocrystalline powders prepared by MA may be consolidated to any desired shape and dimension. However, *all* attempts to prepare a magnetically soft alloy using this method have failed.[8–32] Indeed, the coercivity H_C reported in these studies was on the order of 10^1–10^2 Oe, thus several orders of magnitude higher than those found in nanocrystalline alloys prepared by crystallizing their amorphous precursors.[2,3]

There is no satisfactory explanation for the high coercivity of mechanically alloyed ferromagnetic powders. The present paper studies the various contributions to the coercivity in two mechanically alloyed powders: $Fe_{80}Cu_{20}$ (at. %) and $Fe_{92}Al_2Si_6$ (wt %). For this, we measure the dislocation density and crystallite size as a function of isochronal annealing treatments at increasing temperatures. These two factors are deduced from x-ray diffraction, using the method of Ungar and co-workers,[33–35] which incorporates dislocation contrast factors. We find that the coercivity depends on both crystallite size (as described by the random anisotropy model) and the dislocation density (which controls the residual strains in the alloy). This analysis enables us to modify the random anisotropy model to take into account the effect of residual stress.

II. EXPERIMENT

The alloys were synthesized from elemental Fe (-10 μm, 99.9+ %), Cu (-10 μm, 99.9%), Al (44–149 μm, 99.97%), and Si (chips, 99.9999%). Eight-gram mixtures were mechanically alloyed for 30 h using a SPEX 8000 mill (Edison, NJ) and a hardened-steel vial and balls. Seven ml of hexane was added to the vial to prevent the agglomeration of the powder on the milling media. After evaporating the hexane in a partial vacuum, the powders were transferred to an argon-filled glove box (oxygen content less than 1 ppm). Powder aliquots were annealed for 1 h at various temperatures. The powder was then analyzed by x-ray diffraction (XRD) using Cu $K\alpha$ radiation. NIST silicon standards were used as a reference material which enabled us to accurately determine the position of Bragg reflection peaks and the width of these peaks. The powders were also characterized by scanning electron microscopy (SEM). Small powder

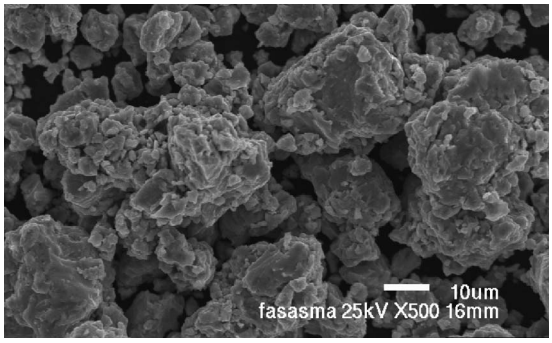

FIG. 1. Scanning electron microscopy image of as-mechanically alloyed $Fe_{92}Al_2Si_6$ (wt %) powder.

samples were hand pressed in aluminum foil capsules, which were used to measure magnetization-field loops using a superconducting quantum interference device (SQUID) at applied fields between −50 and 50 kOe. The magnetic field trapped by the superconducting magnet of the SQUID magnetometer was measured on a platinum standard, and this field was then subtracted from the measurements on our Fe-based powders.

III. RESULTS

Figure 1 is an SEM image of as-mechanically alloyed $Fe_{92}Al_2Si_6$ powder. The particles have quite irregular morphology. The particle size ranges from a few μm to tens of μm. Each particle is an aggregate of smaller micron-size particles. These aggregates are typical of mechanically alloyed powders and result from the repeated cold welding and fracture of powder during ball milling.

Figure 2 shows x-ray diffraction patterns of the $Fe_{80}Cu_{20}$ powders after different thermal treatments. For annealing temperatures below 350 °C, the powder structure is a metastable bcc solid solution, in agreement with a previous study.[36] When annealed at temperatures above 350 °C, fcc Cu precipitates from the bcc solid solutions. Figure 3 shows the diffraction patterns for the $Fe_{92}Al_2Si_6$ powders. The bcc structure of the as-mechanically alloyed Fe(Al, Si) powder is stable even when annealing at a temperature of 650 °C.

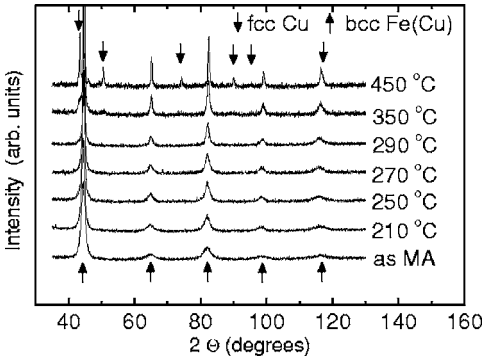

FIG. 2. X-ray diffraction patterns for mechanically alloyed nanocrystalline $Fe_{80}Cu_{20}$ (at. %) powder as a function of annealing temperature (annealing time of 1 h).

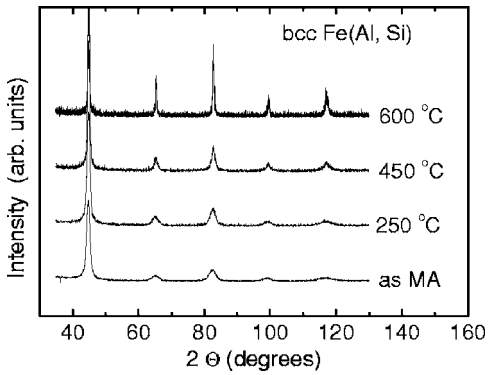

FIG. 3. X-ray diffraction patterns for mechanically alloyed nanocrystalline $Fe_{92}Al_2Si_6$ (wt %) powder as a function of annealing temperature (annealing time of 1 h). All the Bragg peaks are from bcc Fe(Al, Si) solid solutions.

The Bragg diffraction peaks in Figs. 2 and 3 are relatively broad, reflecting a small crystallite size and the presence of residual strain. The two contributions to the broadening are usually analyzed in terms of the Williamson-Hall method,[37] where the width at half maximum (in radian units) of the Bragg peaks, ΔK, is plotted as a function of $K=2\sin\theta/\lambda$. Here θ and λ are the Bragg angle and the wavelength of the x rays, respectively. If the two contributions to the peak profiles are assumed represented by either Cauchy or Gaussian curves, then ΔK is expected to follow the relationships[38]

$$\Delta K = \frac{0.9}{D} + 2eK \quad \text{(Cauchy-Cauchy)}, \tag{1}$$

$$(\Delta K)^2 = \left(\frac{0.9}{D}\right)^2 + 4e^2K^2 \quad \text{(Gaussian-Gaussian)}, \tag{2}$$

where e is lattice strain and D is crystallite size. Figures 4(a) and 4(b) show an analysis of the $Fe_{92}Al_2Si_6$ diffraction data according to Eqs. (1) and (2), respectively. Clearly, the data are not on a straight line, making it difficult to determine the grain size and the residual strain.

Data for nanocrystalline materials often fail to obey the Williamson-Hall plot. The deviations are larger when the material being studied is elastically anisotropic because then the residual strains affect some Bragg reflections more than others. Ungar and co-workers suggested[33–35] methods to take this into consideration through the introduction of a dislocation contrast factor C_{hkl}. Equations (1) and (2) then take the form

$$\Delta K = \frac{0.9}{D} + 2eK\,C^{1/2}, \tag{3}$$

$$(\Delta K)^2 = \left(\frac{0.9}{D}\right)^2 + 4e^2K^2C. \tag{4}$$

The contrast factor for Bragg reflection (hkl), C_{hkl}, can be calculated from the contrast factor for Bragg reflection ($h00$), C_{h00}, according to[35]

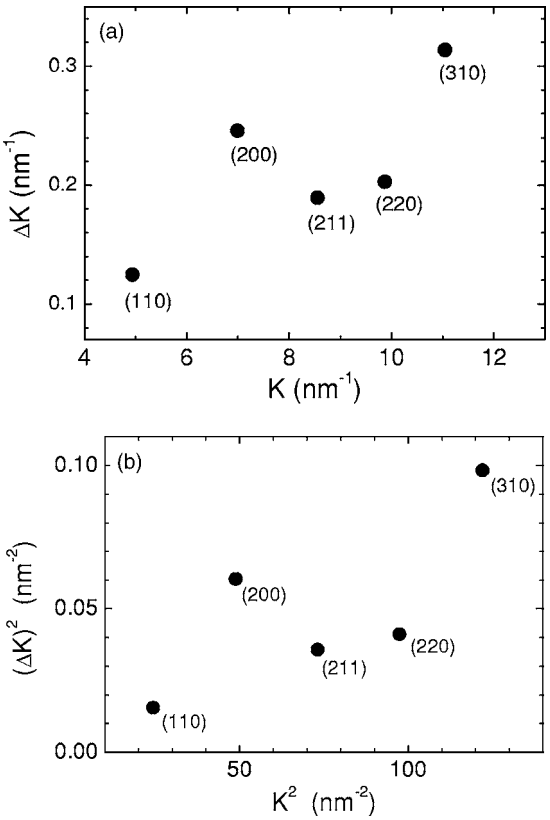

FIG. 4. Williamson-Hall plot for as-mechanically alloyed nanocrystalline $Fe_{92}Al_2Si_6$ (wt %) powder. (a) ΔK-K plot, (b) ΔK^2-K^2 plot.

$$C_{hkl} = C_{h00}(1 - qH^2), \tag{5}$$

where $H^2=(h^2k^2+h^2l^2+k^2l^2)/(h^2+k^2+l^2)$ for a cubic crystal system and q is a constant that is deduced from a fit to the data, as explained below.

For cubic materials, the contrast factor C_{h00} depends on the Burgers and line vectors characterizing the dislocations, the elastic anisotropy S $[S=2C_{44}/(C_{11}-C_{12})]$, and the ratio C_{12}/C_{44} where C_{11}, C_{12}, and C_{44} are the elastic constants.[35] The elastic constants of the present Fe(Cu) and Fe(Al, Si) solid solutions can be approximated by those of pure iron.[39] We used a computer program developed by Borbely *et al.*[40] to calculate the values of C_{h00} for the four different dislocations expected in these alloys: two edge dislocations of $\langle 111\rangle$ $\{110\}$ and $\langle 111\rangle$ $\{211\}$ type and two screw dislocations of $\langle 110\rangle$ and $\langle 111\rangle$ type. We then assumed that the four different dislocation types were present in equal proportion and we thus derived a unique value of C_{h00} by numerically averaging the C_{h00} values calculated for the four dislocation orientations. The averaged value is $C_{h00}=0.252$, which we assumed to represent the C_{h00} value for both Fe-based alloys studied here.

If dislocations are the main contributors to the residual strain, then Eq. (4) can be expressed as[33]

$$(\Delta K)^2 = \left(\frac{0.9}{D}\right)^2 + \left(\frac{\pi b^2 \rho}{2B}\right) K^2 C, \tag{6}$$

where b is modulus of the Burgers vector of dislocations, ρ is the average dislocation density, and B is a constant that can be taken as 10 for a wide range of dislocation distribution.[33] Equations (5) and (6) lead to

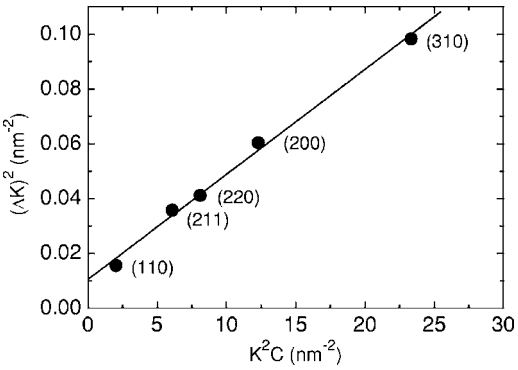

FIG. 5. Modified Williamson-Hall plot (ΔK^2 versus K^2C) for as-mechanically alloyed nanocrystalline $Fe_{92}Al_2Si_6$ (wt %) alloy. C is the average of the dislocation contrast factor, C_{hkl}, for orientation (h,k,l).

$$\frac{(\Delta K)^2 - (0.9/D)^2}{K^2} = \left(\frac{\pi b^2 \rho}{2A}\right) C_{h00}(1 - q\,H^2). \tag{7}$$

Equation (7) is now fitted to the data to deduce the optimal values of D, ρ, and q. To solve this nonlinear fit problem, we followed the suggestion of Ungar *et al.*[34,35] to do a series of *linear* fits of Eq. (7) using a discrete range of $(0.9/D)^2$ values, letting ρ and q vary, and to choose the $(0.9/D)^2$ value that gave the largest correlation coefficient to the fit.

Figure 5 shows the data for the as-mechanically alloyed Fe(Al, Si), plotted according to Eq. (6). In this modified plot, all the Bragg reflections fall on a straight line. The average dislocation density ρ is determined from the slope of the fitted straight line according to Eq. (6) whereas the constant q can be determined from the plot according to Eq. (7). For all the alloys investigated here, q ranged from 1.8 to 3.0.

Figure 6 shows the magnetization-field (M-H) loop for Fe(Al, Si) in the as-mechanically alloyed state. The saturation magnetization M_S measured at an applied field of 50 kOe is 186.5 emu/g, corresponding to approximately

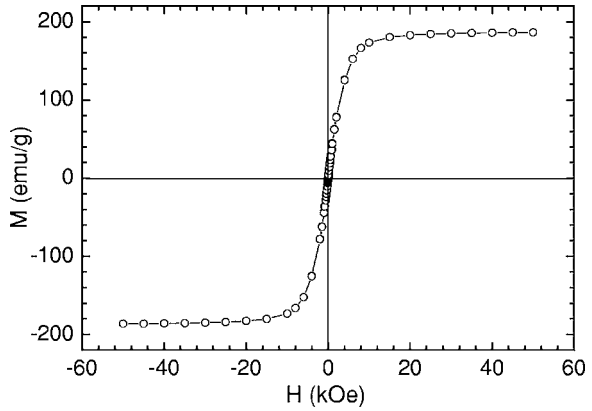

FIG. 6. Magnetization-field, M-H, loops for as mechanically alloyed nanocrystalline $Fe_{92}Al_2Si_6$ (wt %) powder. The coercivity is not apparent at the present 60 kOe abscissa scale.

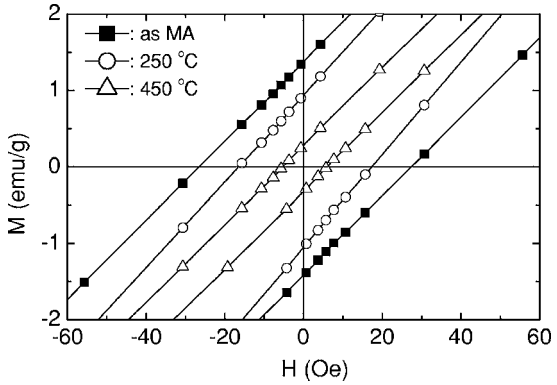

FIG. 7. *M-H* curves, extracted from Fig. 6, for nanocrystalline $Fe_{92}Al_2Si_6$ (wt %) alloys: (■) as mechanically alloyed, (○) after annealed at 250 °C for 1 h, and (△) after annealed at 450 °C for 1 h. The field has been corrected to take into account the field trapped in the SQUID.

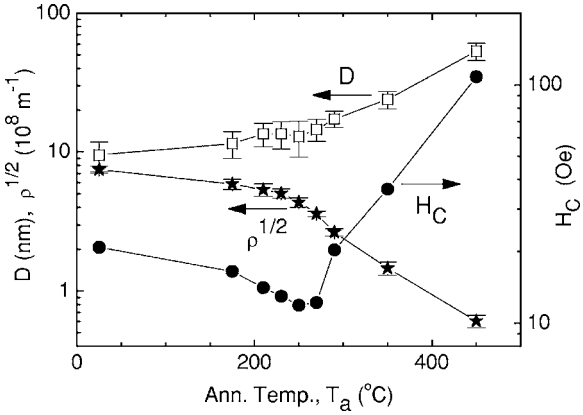

FIG. 8. Coercivity H_C, crystallite size D, and square root of dislocation density, $\rho^{1/2}$, as a function of annealing temperature T_a for mechanically alloyed nanocrystalline $Fe_{80}Cu_{20}$ (at. %) powder.

1.8 T. This M_S value, when normalized to the content of iron, is 203 emu/g_{Fe}. This value is approximately 9% lower than the saturation magnetization of pure iron. This decrease in magnetization per Fe atom has been attributed[41] to charge transferred from the alloying elements Al and Si to Fe, which partially fills the *d* band of iron and lowers its moment. In our nanocrystalline powders, a large fraction of Fe atoms are located at grain boundaries and thus have larger interatomic distances to their Fe neighbors. This could also contribute to the lowering of the magnetic moment per atom. The susceptibility M/H is small (less than 5). This is because the measurements are done on loose powder consisting of quasi-spherical particles having demagnetizing factor of approximately $4\pi/3$.

Figure 7 shows a magnified view of the *M-H* loops (each measured for a maximum H of 50 kOe) for Fe(Al, Si) in the as-mechanically alloyed condition (solid symbols) and after annealing for 1 h at the stated temperatures (open symbols). To obtain these curves, we first deduce the apparent coercivity of the powders. The true coercivity shown in Fig. 7 was then obtained after subtracting the trapped field measured with a platinum standard.

Figure 8 summarizes the data for the mechanically alloyed $Fe_{80}Cu_{20}$ (at. %), showing the coercivity H_C, crystallite size D, and square root of dislocation density, $\rho^{1/2}$, as a function of the annealing temperature T_a. Upon increasing T_a in the range 20–250 °C, D increases slightly whereas both H_C and $\rho^{1/2}$ decrease. Because for nanocrystalline alloys an increase in D causes a fast increase in H_C, the observed decrease in H_C suggests that in this annealing range the decrease in H_C is dominated by the removal of residual stress, which is usually proportional to $\rho^{1/2}$. H_C reaches a minimum value for T_a=250 °C. Upon increasing the annealing temperature in the range 250–450 °C, D increases and $\rho^{1/2}$ decreases at ever faster rates. However, H_C increases abruptly. This fast increase can be attributed to two factors: (1) the increase of D and (2) the precipitation of fcc Cu from the bcc Fe(Cu) solid solution (Fig. 2). The first factor is explained by the random anisotropy model,[4] which predicts that $H_C \sim D^6$. The second factor is explained qualitatively by the inclusion theory[42] which predicts that H_C is proportional to $N^{2/3}$ where N is the number of nonmagnetic inclusions per unit volume.

Figure 9 shows H_C, D, and $\rho^{1/2}$ as a function of T_a for our $Fe_{92}Al_2Si_6$ (wt %) alloys. The dependence of these parameters on T_a is similar to that seen in Fig. 8, with the exception that the minimum in H_C occurs at 450 °C. Notice also that for temperatures above the minimum, the rate of increase in H_C is larger for $Fe_{80}Cu_{20}$ than for $Fe_{92}Al_2Si_6$. This comparison suggests that the fast increase in H_C for $Fe_{80}Cu_{20}$ for $T_a > 250$ °C is mainly due to the precipitation of Cu.

Figure 10 shows H_C as a function of $\rho^{1/2}$ for the $Fe_{80}Cu_{20}$ and $Fe_{92}Al_2Si_6$ alloys. The figures only include data for alloys annealed at temperatures below 250 and 450 °C, respectively, which are the temperatures that give the minimum H_C values. The linear dependence between H_C and $\rho^{1/2}$ can be understood if one considers that within these temperature ranges, D for both alloys remains approximately constant, ranging from ~9 to 13 nm, and thus the value of H_C is dominated by the dislocation density ρ. Notice that an extrapolation of the data to zero dislocation density gives $H_C \approx 0$.

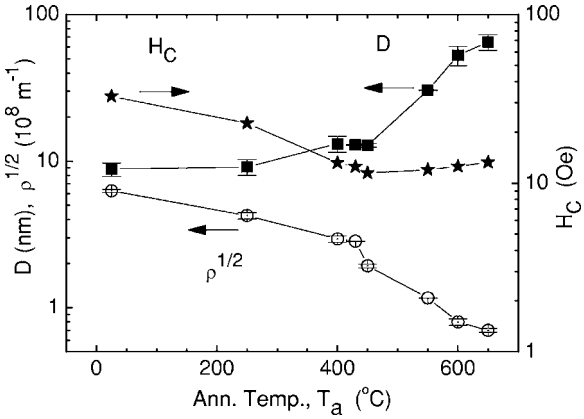

FIG. 9. Coercivity H_C, crystallite size D, and square root of dislocation density, $\rho^{1/2}$, as a function of annealing temperature T_a for mechanically alloyed nanocrystalline $Fe_{92}Al_2Si_6$ (wt %) powder.

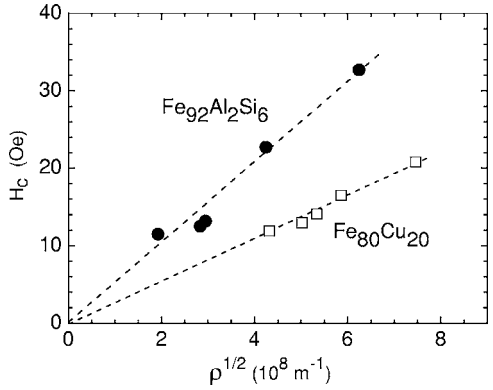

FIG. 10. Coercivity H_C as a function of square root of dislocation density, $\rho^{1/2}$, for mechanically alloyed nanocrystalline $Fe_{80}Cu_{20}$ (at. %) and $Fe_{92}Al_2Si_6$ (wt %) powder, both of similar grain size $D \sim 10$ nm.

IV. DISCUSSION

A. Random anisotropy model in the absence of residual stress

Alben *et al.*[5] proposed a random anisotropy model to describe the ferromagnetism in metallic glasses. Herzer[4] modified this model to explain the soft magnetic properties of nanocrystalline alloys. Herzer's model explains adequately the magnetic properties of ferromagnetic ribbons prepared by first rapid quenching melt into thin amorphous ribbons, which are then annealed to develop a nanocrystalline structure. Because of the way they are produced, these nanocrystals have low dislocation density and thus low residual stress. In this section we discuss the basic idea of Herzer's model.

When grain size D is smaller than the exchange length L_{ex}, the *effective* anisotropy $\langle K \rangle$ of the nanocrystalline material is smaller than the crystalline anisotropy constant K_1. The effective anisotropy is an average of K_1 over the N grains within the volume $V = L_{ex}^3$—i.e.,

$$\langle K \rangle = \frac{K_1}{\sqrt{N}}, \tag{8}$$

where

$$N = \frac{L_{ex}^3}{D^3}. \tag{9}$$

The exchange length L_{ex} can then be expressed as

$$L_{ex} = \sqrt{\frac{A}{\langle K \rangle}}, \tag{10}$$

where A is the exchange stiffness constant. From Eqs. (8), (9), and (10) one obtains[4]

$$\langle K \rangle = \frac{K_1^4}{A^3} D^6. \tag{11}$$

A is related to the spin-wave stiffness constant D_0 by[43,44]

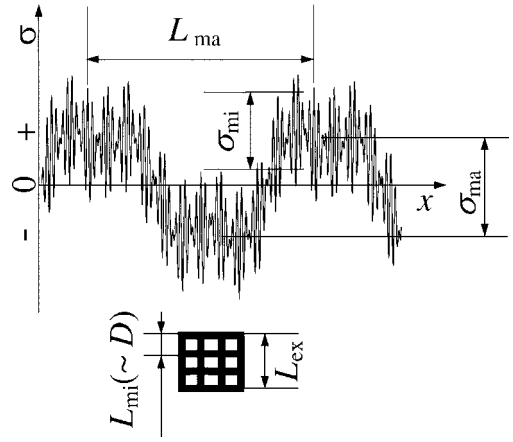

FIG. 11. Schematic representation of the residual stress along an arbitrary direction within a mechanically alloyed powder particle. The length scale of the microstress is $L_{mi} \approx D \approx 10$ nm. The length scale of the macrostress is $L_{ma} \approx$ aggregate thickness ≈ 1 μm. Soft ferromagnetism requires the size D to be smaller than the exchange length L_{ex}, as shown in the figure.

$$A = \frac{D_0 M_S}{2 g \mu_B}, \tag{12}$$

where M_S is saturation magnetization, g is a g factor, and μ_B is Bohr magneton. The M_S for the $Fe_{92}Al_2Si_6$ alloys is 186 ± 3 emu/g $\approx 1.4 \times 10^6$ A/m. Using the D_0 value measured for crystalline $Fe_{93.5}Si_{6.5}$ (wt %),[45] $D_0 = 230$ (meV Å^2) $= 3.68 \times 10^{-40}$ J m^2, and the $g = 2.09$ value for crystalline Fe,[46] Eq. (12) gives $A = 1.3 \times 10^{-11}$ J/m. For crystalline $Fe_{93.5}Si_{6.5}$ (wt %) with $K_1 = 2.2 \times 10^4$ J/m^3[47] and $D = 10$ nm, Eq. (11) gives $\langle K \rangle = 1.1 \times 10^2$ J/m^2, approximately two orders of magnitude smaller than K_1. Because $H_C \propto \langle K \rangle$,[4] the decrease in the anisotropy from K_1 to $\langle K \rangle$ explains why stress-free nanocrystalline alloys are magnetically soft. The random anisotropy model, as discussed above, does not include the effect of residual stresses. In the following sections we modify this model to include the effect of residual stresses, which are prevalent in our mechanically alloyed powders.

B. Random anisotropy model in the presence of residual stress

Our mechanically alloyed powders have high dislocation densities, on the order of 10^{15}–10^{17} m^{-2}, as shown in Figs. 8 and 9. The effect of the residual stress on the total magnetic anisotropy cannot be neglected.

Figure 11 gives a schematic description on the residual stress in a mechanically alloyed particle as a function of distance x inside the particle. This description is consistent with the morphology of the present powders (Fig. 1) and our current understanding of the mechanical alloying process. The fluctuating internal stress has a macroscopic-range component σ_{ma} and a microscopic-range component σ_{mi}. The wavelength of the macrostress, L_{ma}, is on the order of 1 μm, which is approximately the size of aggregates forming each particle in Fig. 1. The wavelength of microstress, L_{mi}, is approximately equal to crystallite size D, which is assumed

here to be smaller than the exchange length L_{ex}. In nanocrystalline alloys prepared by mechanical alloying, the grain boundaries are relatively diffuse and contain a high density of tangled dislocations, leading to high-frequency fluctuations in the microscopic stress.

The stresses σ_{ma} and σ_{mi} produce magnetoelastic anisotropy $K_{\sigma,ma}$ and $K_{\sigma,mi}$ according to[48]

$$K_{\sigma,ma} = \frac{3}{2}\lambda_S \sigma_{ma}, \tag{13}$$

$$K_{\sigma,mi} = \frac{3}{2}\lambda_S \sigma_{mi}, \tag{14}$$

where λ_S is saturation magnetostriction. Both $K_{\sigma,ma}$ and $K_{\sigma,mi}$ contribute to the total effective anisotropy.

The total (effective) anisotropy K_{eff} of a nanocrystalline alloy with a residual stress such as that shown schematically in Fig. 11 has three contributions: the long-range magnetoelastic anisotropy $K_{\sigma,ma}$, the averaged short-range magnetoelastic anisotropy $\langle K_{\sigma,mi}\rangle$, and the averaged short-range magnetocrystalline anisotropy $\langle K_1\rangle$:

$$K_{eff} = \sqrt{K_{\sigma,ma}^2 + \langle K_{\sigma,mi}\rangle^2 + \langle K_1\rangle^2}. \tag{15}$$

Using Eq. (14) and in analogy to Eq. (8),

$$\langle K_{\sigma,mi}\rangle = \frac{\frac{3}{2}\lambda_S \sigma_{mi}}{\sqrt{N}}. \tag{16}$$

Then, from Eqs. (8)–(10), (13), and (16), we obtain an implicit relation for K_{eff}:

$$K_{eff} = \sqrt{\left(\frac{3}{2}\lambda_S \sigma_{ma}\right)^2 + \left[\left(\frac{3}{2}\lambda_S \sigma_{mi}\right)^2 + K_1^2\right]\frac{D^3 K_{eff}^{3/2}}{A^{3/2}}}. \tag{17}$$

It is interesting to asses the analytical dependence of K_{eff} for limiting values of residual stress and magnetostriction.

For $\rho \approx 0$, which means that σ_{ma} and σ_{mi} are both negligible, the value of K_{eff} predicted by Eq. (17) reverts to that predicted by Herzer's random anisotropy model, Eq. (11). The same K_{eff} value is predicted for the case that $\lambda_S = 0$.

The present study shows that for $\rho \gg 0$ and $\lambda_S \neq 0$, the value of K_{eff} is dominated by the first term in the square root of Eq. (17). The residual stress in heavily deformed materials is an appreciable fraction of the flow stress σ_{flow}, which we estimated from the microhardness of the alloy, H_V. For as-mechanically alloyed $Fe_{92}Al_2Si_6$ we measured $H_V \sim 8$ GPa. The flow stress is approximately equal to $H_V/3 = 2.7$ GPa. The same flow stress follows from the known work-hardening expression $\sigma_{flow} = \alpha G b \sqrt{\rho}$, where α is a parameter in the range 0.2–0.3,[49] $G = 81.6$ GPa is the shear modulus, and b is the length of the Burgers vector. For bcc iron crystals, $b = \sqrt{3}/2\ a = 0.248$ nm where a is a lattice constant. With $\alpha = 0.25$ and the $\rho = 3.9 \times 10^{17}$ (m^{-2}) value we deduced from x-ray diffraction measurement (Fig. 9), we obtain $\sigma_{flow} = 3.2$ GPa which is in good agreement with the value deduced from the hardness measurement. In what follows we assume $\sigma_{ma} \approx \sigma_{flow}$. Then, with $\lambda_S = 2 \times 10^{-6}$ (Ref. 50] we obtain $K_{eff} \approx \frac{3}{2}\lambda_S \sigma_{ma} = 9 \times 10^3$ (J m^2). Finally, using the relation[4]

$$H_C = p_c \frac{K_{eff}}{M_S}, \tag{18}$$

with the parameter p_c set to 0.13 to 0.64,[4] we obtain H_C of 8–41 Oe, which is in reasonable agreement with the measured value of 33 Oe (Fig. 9).

In summary, Eq. (17) predicts that the coercivity in nanocrystalline materials ($D \ll L_{ex}$) depends on both dislocation density and crystallite size. Four limiting cases can be envisaged:

$$\text{case 1:} \quad |\lambda_S| \to 0, \quad \rho \to 0, \quad H_C \propto D^6,$$

$$\text{case 2:} \quad |\lambda_S| \to 0, \quad \rho \gg 0, \quad H_C \propto D^6,$$

$$\text{case 3:} \quad |\lambda_S| \gg 0, \quad \rho \to 0, \quad H_C \propto D^6,$$

$$\text{case 4:} \quad |\lambda_S| \gg 0, \quad \rho \gg 0, \quad H_C \propto \sqrt{\rho},$$

The D^6 dependence can *only* be observed when either λ_S or ρ or both are nearly zero. For alloys containing a large dislocation density, as obtained after mechanical alloying or equal-channel angular extrusion, H_C is dominated by the *long-range* residual stresses generated by dislocations (case 4). By long-range we mean stress fluctuations over a length scale that is larger than the crystallite size and also larger than the exchange length, L_{ex}. The presence of these long-range stresses destroys all the advantages of having nanosized grains, forcing the nanocrystalline material to behave as a conventional large grain material.

From the present work we conclude that nanocrystalline powders prepared by mechanical alloying are magnetically soft only if they are either nonmagnetostrictive ($|\lambda_S| \to 0$) or dislocation free ($\rho \to 0$). Zero magnetostriction can be achieved in some alloy systems [e.g., Fe-Si (Ref. 51)], but at the expense of limiting the alloy composition. The second path ($\rho \to 0$) is more difficult to follow because a thermal anneal aimed at reducing ρ will also tend to cause grain growth (as revealed in Figs. 8 and 9). However, this path could be followed by first preparing amorphous alloys (using the mechanical alloying technique) and then optimally annealing the amorphous precursors. The high-temperature anneal would produce amorphous or nanocrystalline alloys in which most of the residual stress is annealed out. The main advantage of using mechanical alloying to prepare the amorphous precursor is that the alloy composition is not limited to that of deep eutectics.

V. CONCLUSIONS

(i) The Williamson-Hall method, frequently used to deduce the residual strain and grain size of deformed solids, is inappropriate for analyzing powders of elastically anisotropic materials. A proper analysis requires the introduction of dislocation contrast factors that take into account the elastic anisotropy.

(ii) In nanocrystalline powders prepared by mechanical alloying, the coercivity is a nonlinear function of the grain size and the residual stress within the particles. At low annealing temperatures the coercivity decreases because of the fast removal of long-range residual stress whereas at higher annealing temperatures the coercivity increases because annealing causes grain growth. For $Fe_{80}Cu_{20}$ (at. %) and $Fe_{92}Al_2Si_6$ (wt %) studied here, there is an optimum annealing temperature (250 and 450 °C, respectively) at which the coercivity is lowest.

(iii) Below the optimum annealing temperature, the coercivity is a linear function of the square root of the dislocation density. The high-density dislocations cannot be completely removed by annealing while avoiding grain growth.

(iv) The total anisotropy in a nanocrystalline powder prepared by mechanical alloying has three contributions: (1) long-range magnetoelastic anisotropy, (2) random short-range magnetoelastic anisotropy, and (3) random short-range magnetocrystalline anisotropy. The last two contributions are proportional to the sixth power of the crystallite size and thus are unimportant in mechanically alloyed powders with crystallite size $D \ll L_{ex}$. The main contribution to the coercivity of nanocrystalline alloys arises from the fluctuating long-range residual stress which is proportional to the square root of the dislocation density.

ACKNOWLEDGMENTS

This work was supported by the Office of Freedom Car and Vehicle Technologies of the U.S. Department of Energy. We are grateful to program manager Dr. Sidney Diamond for his support and encouragement. The authors thank Dr. Tamas Ungar for discussions on the fitting of x-ray diffraction profiles.

*Corresponding author. Current address: Structure-Property Relationship Group, MST-8, Mail Stop G755, Materials Science and Technology Division, Los Alamos National Laboratory, Los Alamos, NM 87545, USA. FAX: (505) 667-8021. Electronic address: tdshen@lanl.gov

[1] Y. Yoshizawa, S. Oguma, and K. Yamauchi, J. Appl. Phys. **64**, 6044 (1988).
[2] G. Herzer, in *Handbook of Magnetic Materials*, edited by K. H. J. Buschow (Elsevier Science B.V., Amsterdam, 1997), Vol. 10, Chap. 3.
[3] M. E. McHenry, M. A. Willard, and D. E. Laughlin, Prog. Mater. Sci. **44**, 291 (1999).
[4] G. Herzer, IEEE Trans. Magn. **26**, 1397 (1990).
[5] R. Alben, J. J. Becker, and M. C. Chi, J. Appl. Phys. **49**, 1653 (1978).
[6] K. Lu, Mater. Sci. Eng., R. **16**, 161 (1996).
[7] B. S. Murty and S. Ranganathan, Int. Mater. Rev. **43**, 101 (1998).
[8] N. Kataoka, K. Suzuki, A. Inoue, and T. Masumoto, J. Mater. Sci. **26**, 4621 (1991).
[9] T. D. Shen, K. Y. Wang, M. X. Quan, and J. T. Wang, J. Mater. Sci. Lett. **11**, 1576 (1992).
[10] C. Kuhrt and L. Schultz, IEEE Trans. Magn. **29**, 2667 (1993).
[11] C. Kuhrt and L. Schultz, J. Appl. Phys. **73**, 6588 (1993).
[12] A. Hernando, P. Crespo, J. M. Barabdiaran, A. García Escorial, and R. Yavari, J. Magn. Magn. Mater. **124**, 5 (1993).
[13] P. Crespo, A. Hernando, R. Yavari, O. Drbohlav, A. García Escorial, J. M. Barandiarán, and I. Orúe, Phys. Rev. B **48**, 7134 (1993).
[14] O. Drbohlav and A. R. Yavari, J. Magn. Magn. Mater. **137**, 243 (1994).
[15] O. Drbohlav and A. R. Yavari, Acta Metall. Mater. **43**, 1799 (1995).
[16] C. Kuhrt, J. Magn. Magn. Mater. **157/158**, 235 (1996).
[17] R. Schäfer, S. Roth, C. Stiller, J. Eckert, U. Klement, and L. Schultz, IEEE Trans. Magn. **32**, 4383 (1996).
[18] C. Stiller, J. Eckert, S. Roth, R. Schäfer, U. Klement, and L. Schultz, Mater. Sci. Forum **225–227**, 695 (1996).
[19] B. Majumdar, M. M. Raja, A. Narayanasamy, and K. Chattopadhyay, J. Alloys Compd. **248**, 192 (1997).
[20] H. N. Frase, R. D. Shull, L.-B. Hong, T. A. Stephens, Z.-Q. Gao, and B. Fultz, Nanostruct. Mater. **11**, 987 (1999).
[21] C. N. Chinnasamy, A. Narayanasamy, K. Chattopadhyay, and N. Ponpandian, Nanostruct. Mater. **12**, 951 (1999).
[22] Y. D. Kim, J. Y. Chung, J. Kim, and H. Jeon, Mater. Sci. Eng., A **291**, 17 (2000).
[23] M. Kis-Varga, D. L. Beke, and L. Daróczi, Mater. Sci. Forum **343–346**, 841 (2000).
[24] J. Ding, Y. Li, L. F. Chen, C. R. Deng, Y. Shi, Y. S. Chow, and T. B. Gang, J. Alloys Compd. **314**, 262 (2001).
[25] Y. J. Liu, I. T. H. Chang, and M. R. Lees, Scr. Mater. **44**, 2729 (2001).
[26] J. Ding, Y. Shi, L. F. Chen, C. R. Deng, S. H. Fuh, and Y. Li, J. Magn. Magn. Mater. **247**, 249 (2002).
[27] T. Mashimo, X. Fan, X. S. Huang, H. Murata, and M. Sakakibara, J. Phys.: Condens. Matter **14**, 10825 (2002).
[28] N. E. Fenineche, R. Hamzaoui, and O. El Kedim, Mater. Lett. **57**, 4165 (2003).
[29] B. H. Lee, B. S. Ahn, D. G. Kim, S. T. Oh, H. Jeon, J. Ahn, and Y. D. Kim, Mater. Lett. **57**, 1103 (2003).
[30] R. Hamzaoui, O. Elkedim, N. Fenineche, E. Gaffet, and J. Craven, Mater. Sci. Eng., A **360**, 299 (2003).
[31] E. Fechova, P. Kollar, J. Fuzer, J. Kovac, P. Petrovic, and V. Kavecansky, Mater. Sci. Eng., A **107**, 155 (2004).
[32] R. Hamzaoui, O. Elkedim, and E. Gaffeet, Mater. Sci. Eng., A **381**, 363 (2004).
[33] A. Revesz, T. Ungar, A. Borbely, and J. Lendvai, Nanostruct. Mater. **7**, 779 (1996).
[34] T. Ungar and G. Tichy, Phys. Status Solidi A **171**, 425 (1999).
[35] T. Ungar, I. Dragomir, A. Revesz, and A. Borbely, J. Appl. Crystallogr. **32**, 992 (1999).
[36] J. Eckert, J. C. Holzer, and W. L. Johnson, J. Appl. Phys. **73**, 131 (1993).
[37] G. K. Williamson and W. H. Hall, Acta Metall. **1**, 22 (1953).
[38] H. P. Klug and L. E. Alexander, in *X-ray Diffraction Procedures for Polycrystalline and Amorphous Materials* (Wiley, New York, 1974), p. 661.

[39] C. J. Smithells, *Metals Reference Book*, 5th ed. (Butterworths, London, 1976), p. 978.
[40] A. Borbely, J. Dragomir-Cernatescu, G. Ribarik, and T. Ungar, J. Appl. Crystallogr. **36**, 160 (2003).
[41] K. Yamauchi and T. Mizoguchi, J. Phys. Soc. Jpn. **39**, 541 (1975).
[42] A. H. Morrish, in *the Physical Principles of Magnetism* (Krieger, Huntington, NY, 1980), p. 389.
[43] M. Vazquez, W. Fernengel, and H. Kronmüller, Phys. Status Solidi A **115**, 547 (1989).
[44] J. Weissmuller, R. D. McMichael, A. Michels, and R. D. Shull, J. Res. Natl. Inst. Stand. Technol. **104**, 261 (1999).
[45] J. W. Lynn, Phys. Rev. B **11**, 2624 (1975).
[46] B. E. Argyle, S. H. Charap, and E. W. Pugh, Phys. Rev. **132**, 2051 (1963).
[47] H. Gengnagel and H. Wagner, Z. Phys. **8**, 174 (1961).
[48] B. D. Culity, *Introduction to Magnetic Materials* (Addison-Wesley, Reading, MA, 1972), pp. 266–274.
[49] A. S. Argon, in *Physical Metallurgy*, 4th ed., edited by R. W. Cahn and P. Haasen (Elsevier Science B.V., Amsterdam, 1996), Chap. 21.
[50] M. Takahashi, N. Kato, T. Sato, and T. Wakiyama, IEEE Trans. Magn. **23**, 3068 (1987).
[51] Y. Shimada and H. Kojima, J. Appl. Phys. **47**, 4156 (1976).